2D NMR Studies and 3D Structure of the Parallel-Stranded Duplex Oligonucleotide Acrm$_5$-α-d(TCTAAACTC)-β-d(AGATTTGAG) via Complete Relaxation Matrix Analysis of the NOE Effects and Molecular Mechanics Calculations

J.-L. Guesnet, F. Vovelle, N. T. Thuong, and G. Lancelot*

Centre de Biophysique Moléculaire, CNRS, 45071 Orléans Cédex 2, France

Received June 6, 1989; Revised Manuscript Received December 14, 1989

ABSTRACT: The three-dimensional structure of the duplex formed by the association of the unnatural oligonucleotide α-d(TCTAAACTC) covalently linked to an acridine derivative (m$_5$Acr) with its natural and parallel complementary sequence β-d(AGATTTGAG) was investigated by nuclear magnetic resonance spectroscopy and constrained molecular mechanics calculations. All the nonexchangeable and exchangeable resonances were assigned in this duplex. The structure was refined by using interproton distances determined by NOE measurements. The NOE values were converted into distances by using the complete 190 × 190 relaxation matrix. The unnatural duplex Acrm$_5$-α-d(TCTAAACTC)-β-d(AGATTTGAG) forms a parallel right-handed helix with Watson-Crick base pairing; the α and β deoxyriboses adopt a 3'-exo conformation. The acridine moiety was found stacked up the C9-G9 base pair. The structure of the first seven base pairs of this duplex was found similar to that of the duplex α-d(TCTAAAC)-β-d(AGATTTG), which we had already investigated [Lancelot, G., et al. (1989) *Biochemistry 28*, 7871-7878]. Since these structures were generated by using experimental NOE values obtained independently on macromolecules whose global correlation time was different (3.8 and 2.2 ns), we conclude that this comparison is a good test of the viability of our method to generate three-dimensional structures of oligonucleotides in solution. Starting from different initial conformations, we show that the NOE constraints allow one to reach the same final restrained conformation, taking into account implicitly the solvent effect.

Gene expression can be controlled by a complementary nucleic acid fragment, which binds selectively to the target sequence (Tomazawa & Itoh, 1981; Green et al., 1986). This high and specific process is governed by hydrogen base-pairing formation.

For this purpose, we have synthesized oligodeoxynucleotides covalently linked to an intercalating dye (Asseline et al., 1983, 1984; Hélène et al., 1985; Lancelot et al., 1988). The stability of hybrid formation is strongly increased by covalent attachment of an intercalant agent to an oligodeoxynucleotide (Asseline et al., 1984). In order to increase the resistance of such compounds toward nucleases, α-oligonucleotides were synthesized (Asseline et al., 1986; Morvan et al., 1986; Thuong et al., 1987; Lancelot et al., 1987).

We have recently used nuclear magnetic resonance spectroscopy and constrained molecular mechanics calculations to investigate the three-dimensional solution structure of the parallel α-d(TCTAAAC)-β-d(AGATTTG) duplex (Lancelot et al., 1987, 1989). The duplex adopts a right-helical structure with a Watson-Crick base pairing and sugars in 3'-exo conformation. In order to test the validity of our method, we elucided the three-dimensional structure of an oligonucleotide containing the already studied α-β 7-mer duplex sequence. Two more bases were added on the 3'-end for each strand of the heptamer duplex and a derivative of 9-aminoacridine (2-methoxy-6-chloro-9-aminoacridine) was covalently linked to the 5'-terminal residue of the α-deoxynucleotide via a pentamethylene linker (m$_5$Acr),[1] Acrm$_5$-α-d(TCTAAACTC) (Figure 1). Nuclear magnetic resonance investigation and data analysis conjugated with constrained molecular mechanics enabled us to determine the location of the acridine dye and the three-dimensional solution structure of the unnatural duplex Acrm$_5$-α-d(TCTAAACTC)-β-d(AGATTTGAG). This structure was compared to the structure of the unnatural heptamer already described (Lancelot et al., 1989).

Although input values of NOE effects and correlation times for both duplexes were very different, the final structures were found globally identical for the common sequence.

Experimental Procedures

NMR Spectroscopy. All the investigated compounds were passed through a Chelex-100 column to remove paramagnetic impurities and adjusted to pH 7.0.

NMR experiments were carried out with a Bruker AM-300 spectrometer and processed on an Aspect 3000 computer. The imino proton resonances were observed in H_2O solutions by use of selective composite excitation 1331 proposed by Hore (1983).

The NOESY data were obtained from degassed solutions (3.7 mM in duplex) contained in sealed tubes. Two-dimensional data sets for COSY DQF, NOESY, and HOHAHA spectra were collected in the phase-sensitive mode with the time-proportional phase incrementation scheme (Drobny et al., 1979; Bodenhausen et al., 1980; Marion & Wüthrich, 1983; Marion & Lancelot, 1984). Two-dimensional MLEV 17 HOHAHA experiments were recorded (Bax & Davis, 1985) at several mixing times (27-40 MLEV cycles corresponding to a mixing time of 92-137 ms).

[1] Abbreviations: Acr, 2-methoxy-6-chloro-9-aminoacridine; m$_5$, pentamethylene chain; NOE, nuclear Overhauser effect; NOESY, 2D NOE spectroscopy; COSY DQF, 2D double quantum filtered spectroscopy; AMBER, assisted model building with energy refinement.

0006-2960/90/0429-4982$02.50/0

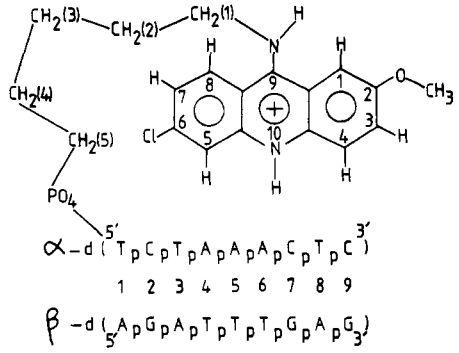

FIGURE 1: Structure of the two oligodeoxyribonucleotides Acrm$_5$-α-d(TCTAAACTC) and β-d(AGATTTGAG). Both parallel strands were numbered from their 5′-terminal residue.

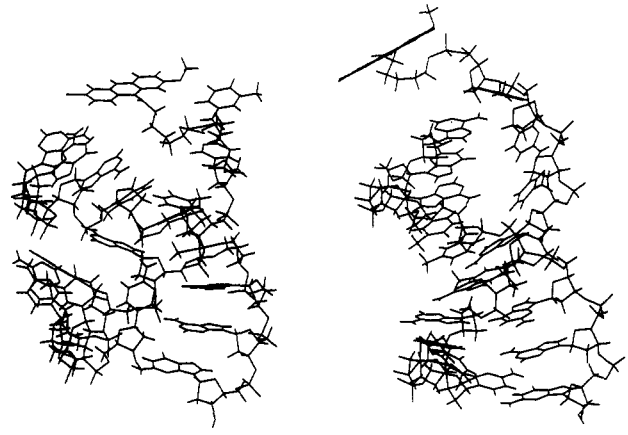

FIGURE 2: View of the two A (left) and B (right) initial conformations of the parallel duplex Acrm$_5$-α-d(TCTAAACTC) and β-d(AGATTTGAG).

Typically, 4096 or 8192 data matrices were collected for each 256 or 384 T_1 values in NOESY, COSY DQF, or HOHAHA experiments. The 512 × 4096 or 1024 × 8192 data matrices were resolution enhanced by a Gaussian window in direction 2 and by a shifted squared "sine-bell" window function in direction 1, then Fourier transformed, and phase adjusted. Volume areas of NOE cross peaks were measured as already described (Lancelot et al., 1989) and compared on several matrix data. Mixing times of 400, 250, 150, 80, 50, 30, 15, and 10 ms were used.

Molecular Mechanics Calculations. The initial conformation was built by generating parallel A and B helix α-d(TCTAAACTC)–β-d(AGATTTGAG) (Figure 2) as already reported (Lancelot et al., 1989). The acridine derivative and the pentamethylene linker were added. Point charges for acridine dye were determined from Cieplak calculations (Cieplak et al., 1987). The chirality of the C1′ atoms of the α-strand was modified in order to set the base in an α-position with respect to the furanose ring. Most of the steric contacts were removed on the Evans and Sutherland PS 390 graphic display by using the FRODO program (Jones, 1978; Pflugrath et al., 1984).

The calculations were carried out on the nonamer Acrm$_5$-α-d(TCTAAACTC)–β-d(AGATTTGAG) using the molecular mechanics program AMBER (Weiner & Kollman, 1981). The various force field parameters and charges used in the calculation for the oligonucleotide were reported previously (Weiner et al., 1984). No counterions were included in the calculation, so the dielectric constant was set equal to $4r_{ij}$ (Weiner et al., 1984). The structures were optimized by using a steepest descent and conjugate gradient algorithm until the rms energy relative to the atomic coordinate changes was less than 0.1 kcal mol^{-1} Å^{-1}.

In a first step, the initial structure has been refined by using AMBER, including distances constraints to ensure the Watson–Crick base pairing. In the next energy minimization, after relaxation of these additional interactions, the NMR constraints were incorporated. For that, an effective harmonic potential representing the interproton constraints was added to the total energy function of the system: $E_{NOE} = K_r(r_{ij} - r_{ij})^2$, where r_{ij} is derived from NMR data. The force constant K_r was chosen to be 25 kcal mol^{-1} Å^{-2} when $r_{ij} < 3$ Å and 15 kcal mol^{-1} Å^{-1} when $r_{ij} > 3$ Å.

RESULTS

Assignment of Resonances and Conformation of the Duplex. The mixing of Acrm$_5$-α-d(TCTAAACTC) with its complementary parallel sequence β-d(AGATTTGAG) leads to upfield shifts and broadening of the resonance lines for both compounds. The temperature dependence of a mixture (3.7 mM of each) of both complementary strands in 0.1 M NaCl shows a melting temperature of 52 °C, while the T_m value for the 7-mer is 33 °C (2 mM duplex, 0.28 M NaCl).

The use of the sequential NOE method for the assignment of nonexchangeable resonances in nucleic acid has been described elsewhere (Hare et al., 1983; Scheek et al., 1983, 1984; Feigon et al., 1983, 1984; Weiss et al., 1984; Wemmer et al., 1984, 1985; Guittet et al., 1984; Broido et al., 1984) and will not be repeated here.

Each H8 or H6 proton of the residues belonging to the β-strand was close to its own H1′ proton and to the H1′ proton of its 5′ neighboring residue, while a similar proximity with the H1′ proton belonging to the 3′ neighboring residue was found for the complementary α-strand (Figure 3), as expected on a right-handed hybrid α–β helix (Lancelot et al., 1987). A similar pathway was found in the H2′/H2″–aromatic protons connectivities (Figure 4). Moreover, the CH_3 of thymines or the H5 protons of cytosines were found connected with the aromatic protons of the 5′ neighboring residue in the β-strand and with the aromatic proton of the 3′ neighboring residue in the α-strand (Figure 4), as already observed in a 7-mer α–β hybrid (Lancelot et al., 1987). We thus concluded that the duplex adopts a right-handed helical structure.

The H2 resonances, characterized by their long T_1 relaxation time, showed some NOE with H1′ protons: β-H2 (A3)–β-H1′ (A3) and β-H2 (A3)–β-H1′ (T4); α-H2 (A4)–α-H1′ (A4) and α-H2 (A4)–βH1′ (T5); α-H2 (A5)–α-H1′ (A5), α-H2 (A5)–α-H1′ (A4), and α-H2 (A5)–β-H1′ (T6); α-H2 (A6)–α-H1′ (A6), α-H2 (A6)–α-H1′ (A6), and α-H2 (A6)–β-H1′ (T6) (Figure 2). All the assignments are given in Table I.

Information about sugar geometry can be obtained from the scalar coupling constants between H1′, H2′, H2″, and H3′. The coupling constants measured on the cross-selectioned COSY DQF matrix were found close to the values obtained for the unnatural heptamer (Lancelot et al., 1987), which is indicative of a 3′-exo conformation of sugars in both strands.

Some weaker NOE were also observed between the H6 or H8 protons of neighboring bases: H8 (A1)–H8 (G2), H8 (G2)–H8 (A3), H8 (A3)–H6 (T4), H6 (T4)–H6 (T5), H6 (T5)–H6 (T6), H6 (T6)–H8 (G7), H8 (G7)–H8 (A8), and H8 (A8)–H8 (G9) for the β-strand and H6 (T1)–H6 (C2), H6 (C2)–H6 (T3), H6 (T3)–H8 (A4), and H8 (A6)–H6 (C7) for the α-strand (Figure 5). All these data are evidence of the formation of a duplex structure with stacked bases.

Hartmann–Hahn spectroscopy could be used to confirm the assignment of sugar protons made on NOESY and COSY

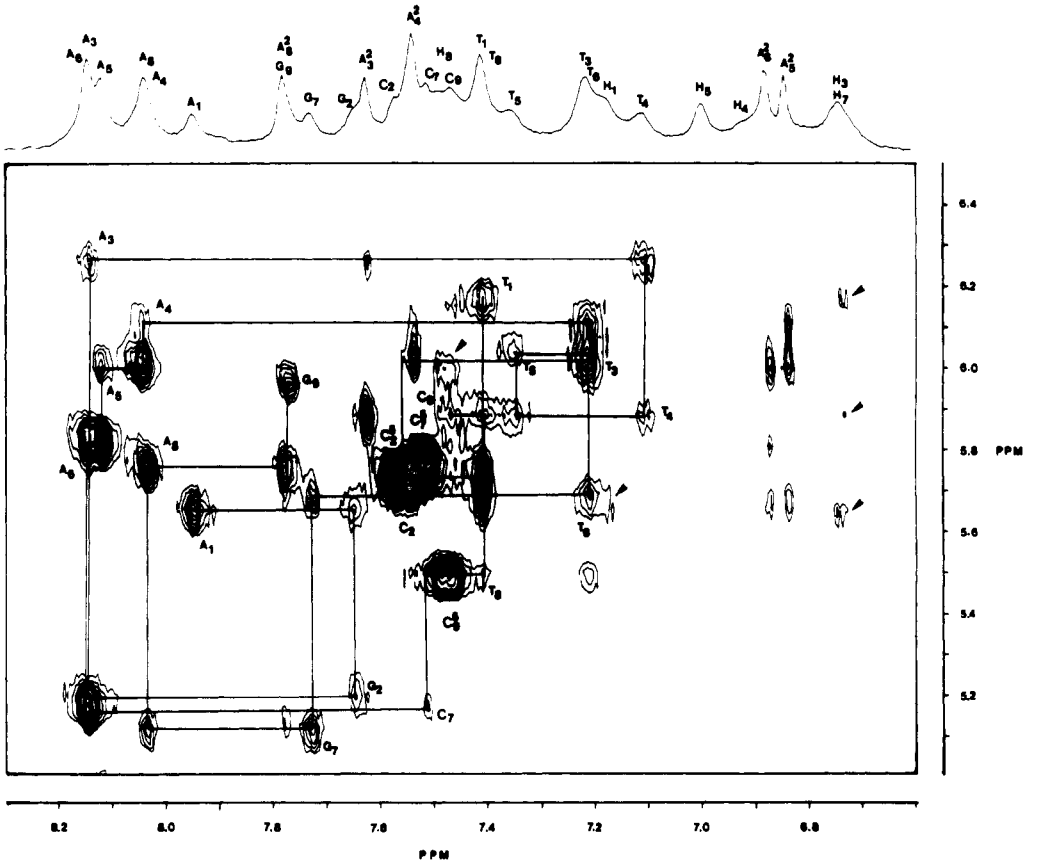

FIGURE 3: Expansion of the aromatic to H1′ proton region of the NOESY spectrum of the duplex $Acrm_5$-α-d(TCTAAACTC)-β-d(AGATTTGAG) (3.7 mM of each) at 30 °C, in 0.1 M NaCl, pH 7.0. H1, H3, H4, H5, H7, and H8 correspond to the acridine protons. Arrows indicate NOE connectivities between duplex and acridine protons.

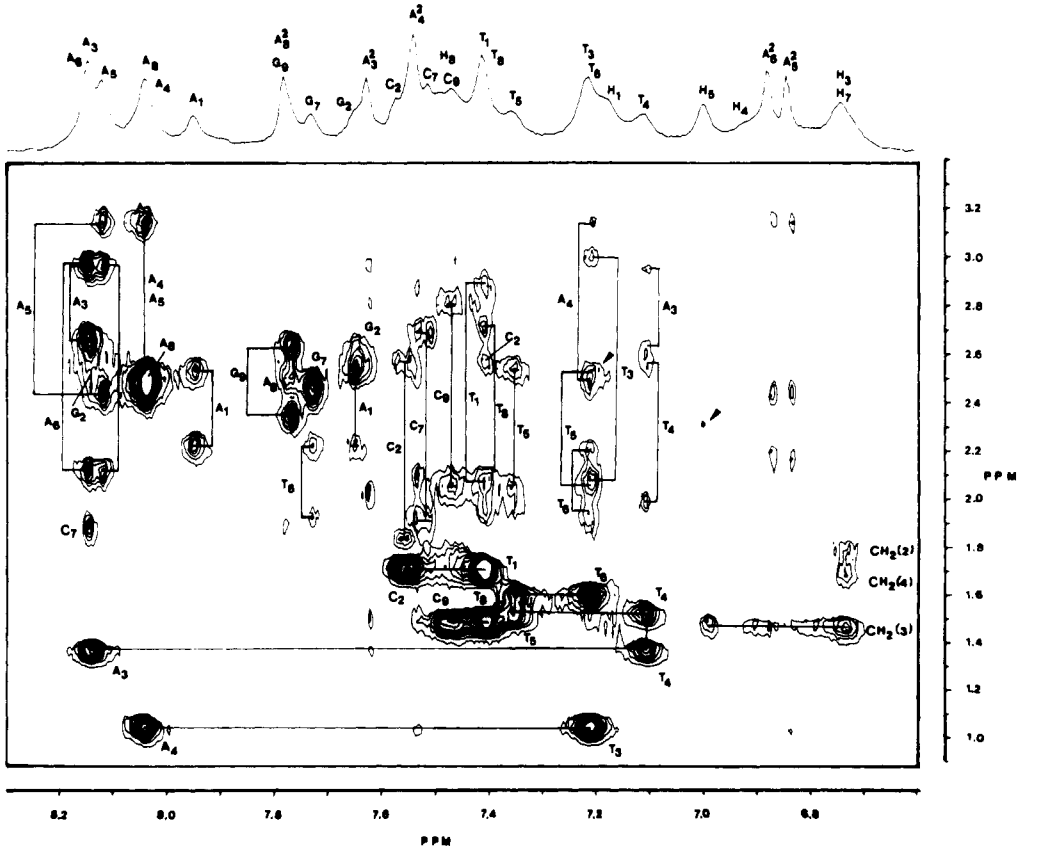

FIGURE 4: Expansion of the aromatic to H2′/H2″ proton region and aromatic to methyl proton region of the NOESY spectrum of the duplex $Acrm_5$-α-d(TCTAAACTC)-β-d(AGATTTGAG) (3.7 mM of each) at 30 °C, in 0.1 M NaCl, pH 7.0. H1, H3, H4, H5, H7, and H8 correspond to the acridine protons. Arrows indicate NOE connectivities between duplex and acridine protons.

Table I: Assignment of the Proton Resonances of the Mini Double Helix Acrm$_5$-α-d(TCTAAACTC)-β-d(AGATTTGAG) (3.7 mM of Each) at 30 °C, in 0.1 M NaCl, pH 7.0[a]

	H8	H6	H5	CH_3	H2	H1′	H2′	H2″	H3′	H4′
T1		7.41		1.73		6.14	2.88	2.12	4.86	4.72
		−0.20		−0.04		−0.07	+0.05	−0.19	0.04	0.04
C		7.56	5.72			5.73	2.69	1.83	4.80	4.39
		−0.08	−0.03			−0.33	−0.19	−0.35	−0.07	−0.34
T3		7.21		1.08		5.98	2.96	2.06	4.82	4.67
		−0.13		−0.17		−0.06	−0.10	−0.09	−0.21	−0.06
A4	8.04				7.54	6.08	3.11	2.44	4.90	4.90
	−0.08				−0.15	−0.10	−0.09	−0.07	−0.13	0.00
A5	8.12				6.84	5.99	3.11	2.44	5.09	4.98
	−0.09				−0.19	−0.09	−0.08	−0.07	−0.08	0.01
A6	8.14				6.88	5.81	2.95	2.13	4.91	4.91
	−0.11				−0.26	−0.11	−0.02	−0.05	−0.04	−0.04
C7		7.52	5.77			5.18	2.66	1.89	4.80	4.80
		−0.06	−0.11			−0.12	0.16	0.20	0.38	0.38
T8		7.41		1.52		5.50	2.70	2.08	4.68	4.68
C9		7.48	5.51			5.88	2.80	2.06	4.66	4.66
A1	7.95					5.67	2.21	2.54	4.80	4.17
	−0.03					−0.16	+0.01	+0.06	+0.07	−0.31
G2	7.65					5.20	2.54	2.54	4.91	4.28
	−0.19					−0.01	−0.14	−0.14	−0.04	−0.02
A3	8.14					6.23	2.61	2.93	5.00	4.45
	−0.14					−0.08	−0.12	−0.02	−0.03	−0.02
T4		7.11	1.40			5.88	2.05	2.54	4.80	4.15
		−0.16	−0.15			−0.09	0.00	−0.04	−0.05	−0.10
T5		7.36	1.54			6.03	2.07	2.44	4.80	4.15
		−0.12	−0.13			−0.09	−0.08	−0.14	−0.04	−0.10
T6		7.21	1.62			5.67	1.92	2.20	4.82	4.17
		−0.13	−0.11			−0.29	−0.01	−0.13	−0.05	−0.08
G7	7.73					5.13	2.43	2.43	4.85	4.17
	−0.18					−0.99	−0.20	0.09	−0.02	0.07
A8	8.04					5.75	2.49	2.49	4.90	4.29
G9	7.78					5.96	2.61	2.33	4.66	4.16

	H1	OCH_3	H3	H4	H5	H7	H8
Acr	7.17	3.55	6.74	6.89	6.99	6.74	7.46

	CH_2 (1)	CH_2 (2)	CH_2 (3)	CH_2 (4)	CH_2 (5)
m_5	3.60	1.80	1.45	1.69	3.90

[a] For each base, the top number refers to the assignment of the nonamer duplex resonances and the bottom number refers to the difference between the chemical shifts of the same resonances measured on the 9-mer and 7-mer.

DQF spectra. On the HOHAHA map, we can see the direct and relayed through-bond connectivities along the H1′–H2′–H2″–H3′–H4′–H5′–H5″ pathway within each sugar moiety and the $CH_2(n)$–$CH_2(n+1)$–$CH_2(n+2)$ pathway within the methylene chain.

Location of the Acridine Derivative. All the protons of the acridine derivative were assigned on the basis of their scalar and dipolar interactions (COSY DQF, HOHAHA, and NOESY maps) (Figure 5). The H7 and H8 resonances were identified by their typical coupling constant, ^3J = 9.0 Hz, on the COSY DQF as well as the H3 and H4 resonances. The H3–H4 doublet was distinguished from the H7–H8 doublet by its connectivity with the methoxy group. The H1 and H5 were identified by their weak NOE with the 2-methoxy group found at 3.55 ppm and the H7 resonance, respectively (Table I). The protons of the methylene chain were assigned from their NOE and scalar connectivities between themselves and with aromatic protons of acridine by assuming that CH_2 (1) rather than CH_2 (5) should present NOE connectivities with the protons of acridine (Figure 4). These assignments (Table I) are supported by the additional connectivities CH_2 (3)–CH_2 (5) and CH_2 (1)–CH_2 (3) corresponding to one-relay coupling observed on the HOHAHA map recorded with a mixing time of 137 ms.

The position of the acridine dye was located by the NOE connectivities of its aromatic protons with the nucleic residues (Figures 2–4). The H7 or H3 acridine proton (6.74 ppm) showed a NOE connectivity with the H6 (T1), H8 (A1), H1′ (T1), and H1′ (A1). Moreover, the H1 (Acr) showed a weak NOE with H1′ (A1) and H2″ (A1). Other NOE were found between the methoxy group protons of acridine and H2′ (T1), H1′ (T1), and H8 (A1) protons of the duplex. Although several NOE were observed between sugar protons of A1 and the OCH_3 of Acr, the overlapping between H5′ (A1) and OCH_3 (Acr) did not allow us to draw any conclusions about the proximity of the aromatic ring to the sugar of A1. These observed NOE between protons of the acridine derivative and protons of the bases and sugars to T1 and A1 pointed out the proximity of the drug to the α-T1–β-A1 base pair. Furthermore, the CH_2 (2)–H1′ (A1) and CH_2 (3)–H1′ (T1) NOE indicated that the pentamethylene linker was close to the T1-A1 base pair.

The acridine dye showed NOE with the T1 moiety on the one hand and with the A1 nucleotide on the other hand. Since all these connectivities cannot exist for a unique conformation of the substituted acridine, we conclude that the dye can adopt two positions, which differ by a 180° rotation of the acridine plane about the N9–C9 bond. The broadening of the aromatic protons of acridine was tentatively explained by exchange between both structures.

Moreover, the NOE connectivities H8 (G9)–H1 (Acr), H8 (G9)–H4 (Acr), H1′ (G9)–H8 (Acr), H1′ (C9)–H3/H7 (Acr), H2′ (C9)–OCH_3 (Acr), and H1′ (G9)–OCH_3 (Acr) and a weak NOE H2″ (G9)–H5 (Acr) pointed out the proximity of the acridine derivative to the C9-G9 base pair.

A NOE was found between OCH_3 (Acr) and H8 (Acr).

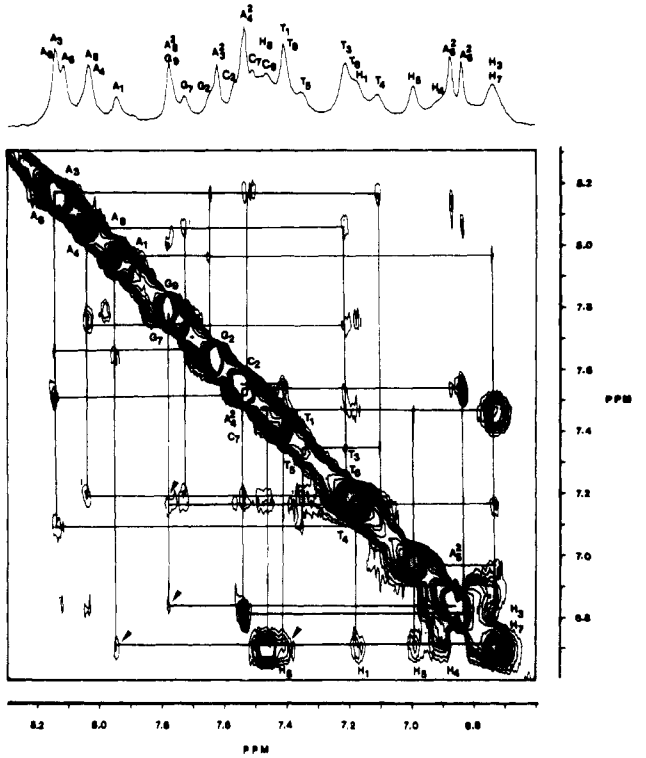

FIGURE 5: Expansion of the aromatic to aromatic proton region of the NOESY spectrum of the duplex $Acrm_5$-α-d(TCTAAACTC)-β-d(AGATTTGAG) (3.7 mM of each) at 30 °C, in 0.1 M NaCl, pH 7.0. H1, H3, H4, H5, H7, and H8 correspond to the acridine protons. Arrows indicate NOE connectivities between duplex and acridine protons.

The distance between OCH_3 and H8 is 7.9 Å; this proximity could be explained by aggregation of two acridine derivatives in an asymmetrical fashion.

Exchangeable Proton Resonances. The imino resonances of the duplex at 4 °C are shown on Figure 6. They were located at 14.01, 13.83, 13.78, 13.66, 13.31, 12.88, 12.57 (2 protons), and 12.53 ppm. The T1-A1 to C7-G7 resonances have the same behavior as those observed for the heptamer duplex (Lancelot et al., 1987). At 36 °C, six enlarged resonances at 13.83, 13.67, 12.95, 12.53 (2 protons), and 12.10 ppm were observed. For the heptamer duplex, all the resonances disappeared at 25 °C, reflecting the difference of stability of both duplexes. Lowering the temperature led to the appearance of more resolved resonances. The N3H (T)–H2 (A) NOE effects are indicative of the Watson–Crick hydrogen bonding of the A-T base pairs (Patel & Hilberts, 1975; Borer et al., 1975).

Generation of the Refined Structure. A first estimation of the proton–proton distances was obtained from the relation $r = r(\text{ref})[\eta(\text{ref})/\eta]^{1/6}$ by using the H6–H5 vector interproton of cytosine as internal reference. All short proton–proton distances (except the distances involving the methyl protons) corresponding to aromatic–sugar intraresidue and interresidue distances, as well as the pseudorotation angles P of sugars, were used for a first constrained energy minimization. The resulting structure allowed us to calculate the new target distances using the complete 190 × 190 relaxation matrix and the relation $r = r(\text{ref})[\eta(\text{ref})/\eta]^{1/6}$ where $r(\text{ref})$ is the distance computed in the refined structure and $\eta(\text{ref})$ the NOE simulated after diagonalization of the relaxation matrix. These new distances were determined by averaging the computed r values for four mixing times (400, 250, 150, and 80 ms) (Lancelot et al., 1989) and were used in the constrained mechanics molecular program for a new iteration.

Table II: Atomic rms between Two Successive Cycles of Refinement (Top), Interproton rms Difference between Initial and Calculated Distances for Each Cycle of Refinement (Middle), and Interproton rms Difference between Two Successive Cycles of Refinement (Bottom)

	cycle of refinement				
	0[a]	1	2	3	4
A starting conformation	3.01	3.79	0.57	0.23	0.09
		0.72	0.59	0.58	0.57
		2.82	0.19	0.11	0.05
B starting conformation	2.47	3.76	0.60	0.40	0.10
		0.68	0.56	0.55	0.54
		1.22	0.17	0.09	0.05

[a] 0 is the initial conformation.

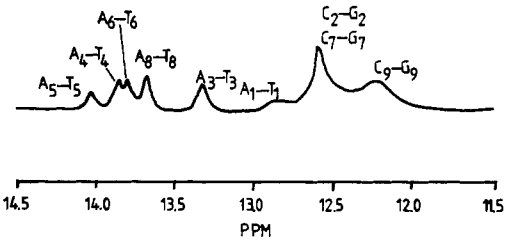

FIGURE 6: Imino proton resonances of the duplex $Acrm_5$-α-d-(TCTAAACTC)-β-d(AGATTTGAG) (3.7 mM of each) at 4 °C in 0.1 M NaCl (pH 7.0) in H_2O/D_2O (4:1).

After three iterations, this process converged and reasonable agreement was found between the calculated and all the experimental interproton distances (92 values) constituting the constraint data base (Table II).

During the last step of the refinement, interproton constraints including protons of the methyl group were added by assuming a free rotation of the methyl group (Lancelot et al., 1989).

The final structure was then reminimized without any constraint leading to a "relaxed" structure. This whole methodology has been reported in detail elsewhere (Lancelot et al., 1989).

The distances of the resulting structure were then compared to the corresponding values for the heptamer and a good agreement was found between both sets of distances for short and long distances.

As already reported for the heptamer duplex (Lancelot et al., 1989), the matrix elements were calculated by assuming an isotropically internal motion for the sugar moiety. A global correlation time of t = 3.75 ns was obtained by fitting the experimental NOE values for H6–H5 of cytosines for different mixing times. A correlation time of 3.2 ns was found for the acridine derivative, using H7–H8 or H3–H4 interproton vector as internal reference (r = 2.46 Å).

Three-Dimensional Structure. Convergence of the Iterative Procedure. Although the initial A and B structures were very different (Figure 2), the two refined structures obtained by using our iterative process were very similar (Figure 7). The atomic root mean square (rms) between the two initial structures was 3.61 Å; it decreased to 0.90 Å after the first iteration and reached 0.39 Å for the two final structures. The atomic rms shifts of the final structures from the initial ones were respectively 3.79 and 3.76 Å. It is worth noting that the iterative procedure led to a rapid convergence toward the final refined structure (Figures 8–10). The atomic rms shifts after each cycle of refinement (rms between the previous and the new refined structures) were 3.79, 0.57, 0.23, and 0.09 for the A initial structure and 3.76, 0.60, 0.40, and 0.10 Å for the B structure (Table II). Simultanously the interproton distance rms differences between two successive steps were 2.82, 0.19,

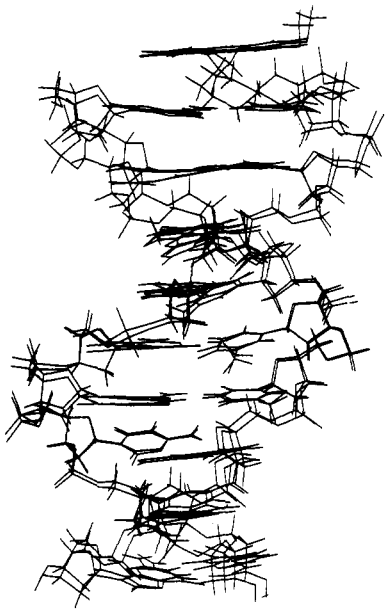

FIGURE 7: View of the superimposition of the two A and B refined structures of the parallel duplex Acrm$_5$-α-d(TCTAAACTC)-β-d-(AGATTTGAG).

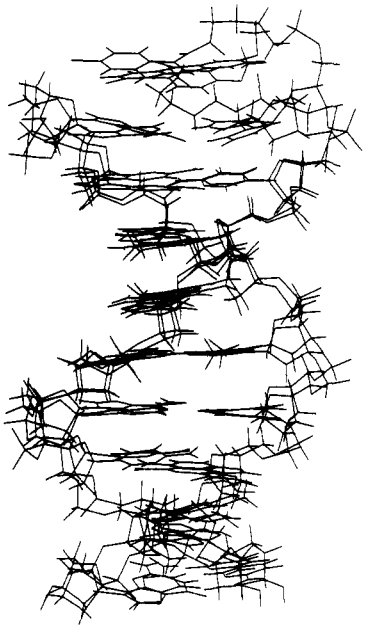

FIGURE 8: View of the superimposition of the two A and B refined structures of the parallel duplex Acrm$_5$-α-d(TCTAAACTC)-β-d-(AGATTTGAG) obtained after the first cycle of refinement.

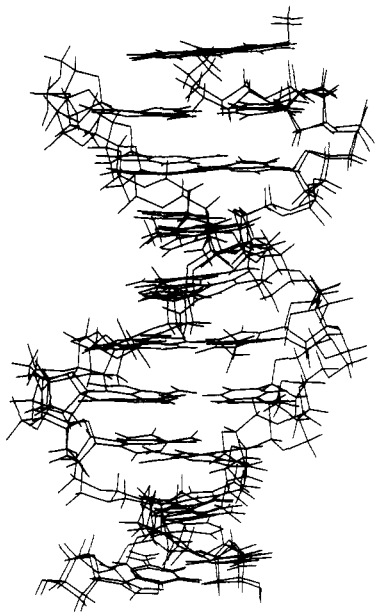

FIGURE 9: View of the superimposition of the A refined structures of the parallel duplex Acrm$_5$-α-d(TCTAAACTC)-β-d(AGATTT-GAG) obtained after the first and the last cycles of refinement. Their atomic rms is 0.78.

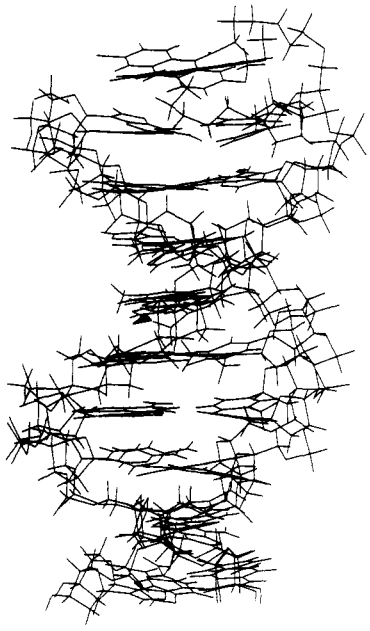

FIGURE 10: View of the superimposition of the B refined structures of the parallel duplex Acrm$_5$-α-d(TCTAAACTC)-β-d(AGATTT-GAG) obtained after the first and the last cycles of refinement. Their atomic rms is 1.16.

0.11 and 0.05 Å for the A form and 1.22, 0.17, 0.09, and 0.05 Å for the B form.

Since the two refined conformations obtained from the A and B structures are very similar, we will only discuss the conformational parameters of the B form, which is more stable by 57 kcal mol^{-1}.

A stereoview of the constrained structure of the duplex is shown in Figure 11. A good agreement between the calculated and experimental interproton distances was obtained (Table III). We can point out that the rms of the base–sugar intraresidue distances (0.10 Å) is the same as the rms of the base–sugar interresidue distances (0.10 Å). All the pseudorotation angles P obtained in the constrained structure are into the range of the experimental data (Table IV).

A stereoview of the superposition of the constrained and relaxed structures is shown on Figure 12.

The average values of the torsion angles and of various helical parameters are given in Tables V and VI. The helical parameters have been calculated by using curves software (Lavery & Sklenar, 1988). Superimposed stereoviews of the final structures of the β-heptamer with Acrm$_5$-α-d-(TCTAAACTC)-β-d(AGATTTGAG) are shown in Figure 13. These structures are globally the same. The torsion angles (α, β, γ, δ, ϵ, and ζ) for each nucleotide unit show little variation between both duplexes. The glycosyl torsion angle (Table V) and the pseudorotation angle P (Table IV) are almost identical between the 7-mer and the 9-mer (Lancelot et al., 1989). As in the α-β heptamer, values of helical twist are alternatively small and large.

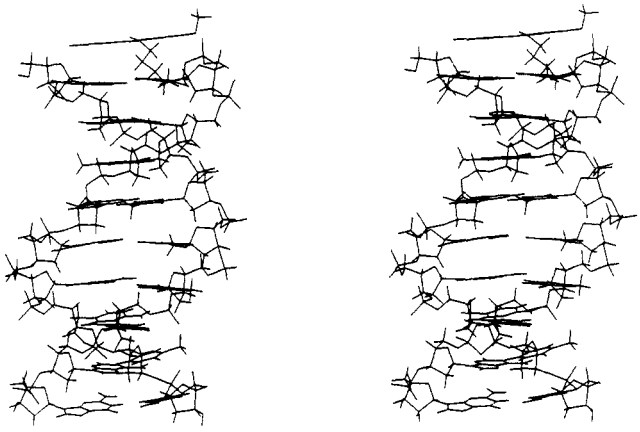

FIGURE 11: Stereoview of the constrained structure of the unnatural duplex Acrm$_5$-α-d(TCTAAACTC)-β-d(AGATTTGAG).

As already pointed out from the NOE experimental data, the acridine derivative can adopt two different positions with respect to the A1-T1 base pair, corresponding to two different set of constraints (Table IIIC).

In a first step the acridine position has been optimized by assuming the first set of constraints. Examination of this structure on the graphic system showed that the second set of constraints can be fulfilled by rotating the acridine dye about the N9–C9 bond. Then, the structure has been reminimized by using this second set of constraints, leading to a structure that is only 20 kcal mol^{-1} less stable than the first one (global energy −520 kcal mol^{-1}). The conformations of the oligonucleotides obtained for these two structures are globally the same; slight differences appear only for the two first pair of bases (Figure 14).

These two structures exhibit the same curvature, 10°, this value being smaller than the corresponding one for the heptamer, 18° (Lancelot et al., 1989).

Discussion

The sequential NOE method assignment of each strand of the parallel 9-mer duplex showed that Acrm$_5$-α-d-(TCTAAACTC)-β-d(AGATTTGAG) adopts a right-handed helical structure. Sugar geometry can be obtained from scalar coupling constants and from aromatic–sugar intraresidue distances. All these data suggest that the sugars adopt a 3′-exo conformation for both strands. The NOE of imino resonances were indicative of Watson–Crick base pairing of the A-T base pairs.

Several NOE connectivities observed between different methylene groups were indicative of the folding of the methylene chain. A set of NOE was observed between the acridine protons and the protons of the A1-T1 base pair, while no NOE were found between the acridine derivative and the C2-G2 base pair. We concluded that the dye was stacked on the top of the T1-A1 base pair. Moreover, the NOE observed between the T1-A1 base-pair protons and several protons of the dye, H1′ (T1)–H3 (Acr), H8 (A1)–H7 (Acr) and H1′ (T1)–H7 (Acr), H8 (A1)–H3 (Acr), showed that the acridine dye can adopt two positions versus the T1-A1 base pair that differ by a 180° rotation about the N9–C9 bond.

Other NOE connectivities found between the dye and the duplex pointed out the proximity of the acridine derivative to the C9-G9 base pair, showing that the dye was sandwiched between the T1-A1 and C9-G9 base pairs belonging to two different duplexes. This conclusion is supported by the fact

Table III: Calculated Distances (Top) and Differences between the Experimental and Calculated Distances (Bottom)

(A) Intranucleotide (H8/H6) with Sugar Atoms

	H1′	H2′	H2″	H4′	H3′	H5′	H5″
α-T1	3.61			3.17			
	−0.13			−0.15			
α-C2		4.15		2.87			
		−0.03		−0.04			
α-T3		3.81	2.66	3.02			
		−0.12	−0.01	−0.04			
α-A4	3.79			3.18			
	−0.05			−0.06			
α-A5	3.72		3.10		4.11		
	−0.16		0.03		−0.06		
α-A6	3.72		3.03	2.96			
	−0.12		−0.03	−0.05			
α-C7	3.65		3.21	2.72			
	−0.04		−0.02	−0.04			
α-T8	3.52			3.04			
	−0.07			−0.02			
β-A1		2.61	4.03			4.42	3.53
		−0.09	−0.06			0.04	−0.02
β-G2	3.85			4.70	4.32		
	−0.01			−0.13	0.04		
β-A3	3.38	2.21	3.75				
	0.47	−0.03	0.08				
β-T4	3.66	2.23	3.44				
	−0.06	0.04	0.03				
β-T5	3.73	2.08	3.43		4.01		
	0.01	0.03	−0.03		−0.07		
β-T6	3.73	2.24	3.58				
	−0.04	0.01	0.04				
β-G7	3.76	2.21			4.06		
	−0.08	0.05			−0.09		
β-A8	3.76						
	−0.08						
β-G9	4.00	2.49	3.91				
	0.02	0.00	0.08				

(B) Internucleotide[a]

	H1′	H2′	H2″	H6/H8	H5/CH$_3$
α-T1	3.37				
	−0.11				
α-C2					3.30[b]
					0.14
α-A4	2.61				3.29[b]
	−0.03				−0.12
α-A5	2.39		4.76		
	0.05		−0.21		
α-A6	2.63		4.92		
	0.02		−0.23		
β-G2	4.18	4.10		6.64[c]	
	0.02	−0.16		−0.16	
β-A3				5.49[c]	3.29[c]
				0.01	0.04
β-T4	3.35	3.56	2.51	4.73[c]	3.28[c]
	−0.03	−0.07	0.08	0.09	0.06
β-T5	3.54			5.26[c]	3.37[c]
	0.01			−0.06	0.01
β-T6	3.55				
	0.00				
β-G7	3.43	4.39	2.62		
	0.01	0.02	0.01		
β-A8	3.71			5.45	
	−0.03			−0.01	
β-G9	3.74		2.75	5.69	
	0.02		0.03	0.00	

(C) Dye–Duplex

	calc	diff
H3 (Acr)–H1′ (T1)	3.61	0.10
H3 (Acr)–H7 (T1)	5.02	−0.02
H7 (Acr)–H8 (A1)	4.03	−0.35

[a] α-Strand (H6/H8) of residue i with atom of residue i + 1. β-Strand (H6/H8) of residue i with atom of residue i − 1. [b] Distances with atom of residue i − 1. [c] Distances with atom of residue i + 1.

Table IV: Calculated P_{theo} and P_{rel} and Differences between P_{theo} for the Heptamer and for the Nonamer[a]

α	P_{theo}	P_{rel}	diff	β	P_{theo}	P_{rel}	diff
T1	215	230	−8	A1	185	159	+2
C2	204	212	+6	G2	187	175	+5
T3	224	223	−5	A3	179	163	+9
A4	214	221	−4	T4	176	124	+4
A5	212	216	0	T5	180	148	−7
A6	205	187	−4	T6	181	161	+2
C7	201	219	−5	G7	189	175	+1
T8	203	205		A8	187	176	
C9	206	236		G9	188	166	

[a] The P_{theo} and P_{rel} values were calculated by running the iterative procedure with and without constraints on the puckering angles P, respectively.

that the global correlation time of the 9-mer (3.75 ns) was much larger than the corresponding value (2.25 ns) already reported for the 7-mer of identical sequence (Lancelot et al., 1989).

A quenching of the fluorescence of the acridine derivative upon binding of the α-oligonucleotide to the parallel β-oligonucleotide has been observed (Sun et al., 1987) and tentatively attributed to a contact with the G2 guanine. Our results do not support this assumption and this quenching should be attributed to the proximity of acridine to the 3′-terminal G9 guanine belonging to another duplex.

A molecular mechanics calculation conjugated with the use of NMR constraints led to a stable structure (−520 kcal mol^{-1}). Although the number of resonances increased as compared to the 7-mer, leading to more severe overlappings and to a relatively smaller number of interproton distances, the agreement found between the calculated and the experimental distances was good, demonstrating that this slight reduction of constraints was not drastic.

Starting from different initial structures (derived from A and B standard conformations), we have shown (Lancelot et al., 1989) that our iterative procedure involving NOE constraints and molecular mechanics calculations led to a unique final structure for the heptamer. The same conclusion was obtained on a monomer duplex linked to an acridine derivative. Moreover, we have shown that starting from two very different sets of NOE values for the 7-mer and the 9-mer, having a common sequence but a different correlation time, our iterative procedure converges to very similar three-dimensional structures for both oligomers. The atomic rms difference for the overlapping 7 base pairs was 0.40 Å and the interproton rms difference was 0.34 Å. These data are consistent with the rms difference (0.43 Å) between the 15 common shortest distances obtained with NOE data at 50 ms for the 7-mer and the 9-mer.

All these results constitute a serious test of reliability of our method.

As already quoted (Lancelot et al., 1989), we did not try to include any solvent molecules in our molecular mechanics calculations. The solvent effects were in fact implicitly taken into account by using NOE data that are recorded in solution.

An energy minimization using the same initial conformation without NOE constraints led to a significantly different final conformation (atomic rms difference 0.85 Å); the interproton distance rms difference between this structure and the constrained one is 0.55 Å.

It is worth noting that the effective harmonic potential term representing the interproton NOE constraints is sufficient to cross the potential barrier in order to reach the optimal structure that satisfied the experimental constraints. A further optimization starting from the constrained refined structure leads to a "relaxed structure" close to this constrained one

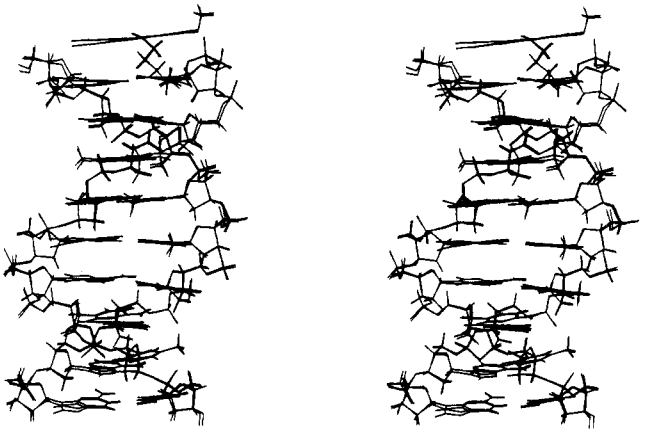

FIGURE 12: Stereoview of the superposition of the constrained and relaxed structures of the unnatural duplex Acrm$_5$-α-d-(TCTAAACTC)-β-d(AGATTTGAG).

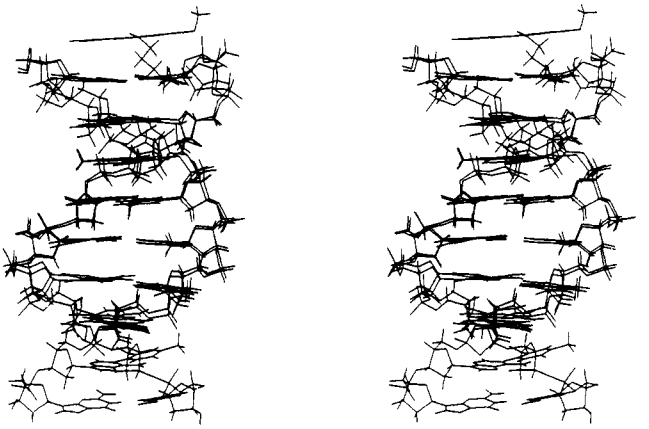

FIGURE 13: Stereoview of the superimposition of the final structures of the α-β heptamer with the Acrm$_5$-α-d(TCTAAACTC)-β-d-(AGATTTGAG) duplex.

(atomic rms difference of 0.39 Å, while the interproton distance rms value between this structure and the unconstrained one is 0.32 Å).

Another important aspect of this study that should be pointed out is the impact of the use of the full relaxation matrix for the distances determination. The rms difference between the distances calculated by using an internal reference and the NOE data obtained at a short mixing time of 50 ms and those calculated by the diagonalization of the full relaxation matrix was 0.35 Å for both final refined structures, but in this evaluation, only the 23 shortest distances corresponding to a NOE intensity superior to 1% were taken into account. For such an oligonucleotide, 23 distances are insufficient to determine the structure without any ambiguity. In order to evaluate the error due to such an approximation, we have used the NOE values obained from the diagonalization of the full relaxation matrix constructed on the final B refined structure and calculated all the distances by using the internal reference H_5–H_6 of cytosine. In this case, the rms difference between these two sets of interproton distances was 0.56 Å. And it must be stressed that by starting with such a set of constraints no convergence can be obtained. In fact, the long distances (H_8–H_2'' on β-anomers and H_8–H_2' on α-anomers) can be erroneous by 0.6–0.8 Å and the sugar conformations cannot be determined with such constraints.

The NOE between protons of sugars (H1′–H2′ and H1′–H2″) were well fitted for different values of mixing times (10–400 ms) with a correlation time of 3.6 ns. The H2′–H2″

Table V: Torsion Angles[a]

α	T1	C2	T3	A4	A5	A6	C7	T8	C9
α		62 69	−98 −94	67 67	−97 −97	−86 −85	−82 −82	−100 −100	−91 −91
β		−121 −118	136 136	−138 −137	139 139	125 124	123 123	174 174	144 144
γ	52 50	−167 −179	48 48	176 178	42 42	48 48	52 51	61 60	44 43
δ	159 170	151 154	148 147	157 156	154 154	147 146	147 147	158 158	156 156
ϵ	−78 −73	−74 −77	−75 −76	−79 −79	−79 −80	−84 −84	−158 −158	−86 −86	
ζ	−176 −176	−165 −162	−172 −172	−162 −163	−167 −167	−175 −175	−122 −122	−165 −165	
χ	119 130	128 133	122 122	134 133	128 128	130 130	136 138	158 159	145 145
α	A1	G2	A3	T4	T5	T6	G7	A8	G9
α		−75 −79	−66 −67	−65 −64	−65 −64	−67 −67	−69 −67	−76 −75	−64 −65
β		174 176	−175 −174	−176 −177	−179 −178	171 174	−179 179	176 177	173 172
γ	70 51	67 67	57 57	51 51	57 55	68 66	55 55	67 66	68 68
δ	145 146	149 149	144 140	137 136	142 142	152 151	147 146	153 153	150 151
ϵ	−154 −152	−177 −177	173 173	−177 −177	−177 −177	−166 −166	−179 −179	−180 −179	
ζ	−124 −125	−112 −110	−92 −92	−116 −115	−114 −114	−131 −133	−107 −107	−123 −124	
χ	−120 −121	−94 −94	−94 −95	−93 −94	−97 −97	−97 −96	−93 −93	−91 −90	−93 −93

[a] Main-chain torsion angles were defined by $P_{\alpha}O5'_{\beta}C5'_{\gamma}C4'_{\delta}C3'_{\epsilon}O3'_{\zeta}P$. χ is the glycosyl bond torsion angle. The two values correspond to both final structures of the Acrm$_5$-α-d(TCTAAACTC)-β-d(AGATTTGAG) nonamer.

Table VI: Helical Parameters for Each Base Step and Propeller Twist for Each Pair of Bases[a]

	twist (deg)	roll (deg)	tilt (deg)
T1–A1			
	36.5	6.9	−9.7
	38.2	8.4	−10.8
	37.3	6.1	−10.0
C2–G2			
	43.2	3.6	8.7
	43.0	0.9	1.5
	41.9	4.1	7.7
T3–A3			
	34.2	2.2	−6.5
	35.6	−7.6	−4.8
	33.3	2.5	−6.9
A4–T4			
	39.4	2.5	1.0
	39.0	2.0	−0.8
	39.5	2.4	1.5
A5–T5			
	37.0	6.5	−0.2
	38.0	−3.8	6.0
	36.3	6.2	−0.6
A6–T6			
	44.8	7.5	−3.5
	45.0	4.2	5.3
	44.7	7.2	−3.3
C7–G7			
	42.0	5.1	−6.2
	42.0	5.1	−6.0
T8–A8			
	43.5	5.2	−0.4
	43.4	4.9	−0.5
C9–G9			
DMP7 (1)	35.9 ± 4.5	−2.3 ± 6.0	0.0 ± 1.5

[a] For each base pair, the first and third values refer to both final structures of the Acrm$_5$-α-d(TCTAAACTC)-β-d(AGATTTGAG) nonamer; the second value is for the α-d(TCTAAAC)-β-d-(AGATTTG) heptamer.

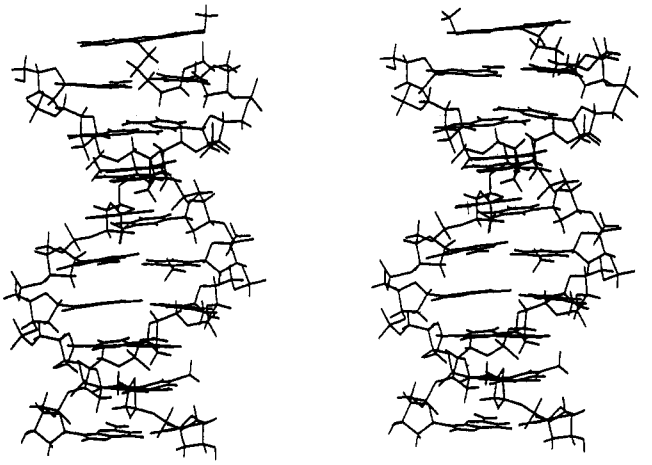

FIGURE 14: Stereoview of the optimized conformation for the Acrm$_5$-α-d(TCTAAACTC)-β-d(AGATTTGAG) nonamer corresponding to the two different positions of the acridine dye.

Table VII: Calculated Distances (Å) and Differences between the Experimental and Calculated Distances between the Methyl Group (H7) and Other Protons[a]

distance	calc	diff
α-H7 (T1)–H6 (C2)	3.30	−0.06
α-H7 (T3)–H8 (A4)	3.29	−0.11
β-H7 (T4)–H8 (A3)	3.29	−0.18
β-H7 (T6)–H6 (T5)	3.37	−0.22
α-H7 (T1)–H4′ (C2)	3.00	0.11
α-H7 (T3)–H1′ (A4)	3.96	−0.11
α-H7 (T3)–H2″ (T3)	5.11	−0.18
β-H7 (T4)–H1′ (A3)	4.79	−0.09
β-H7 (T4)–H2″ (A3)	3.51	−0.01
β-H7 (T4)–H2′ (T4)	4.84	−0.09
β-H7 (T6)–H1′ (T5)	4.30	−0.05
β-H7 (T6)–H2′ (T5)	2.52	0.32
β-H7 (T6)–H2″ (T5)	2.28	0.03

[a] τ_c was computed with H7–H6 as the reference distance.

NOE values could not be used since the 2–3 ppm crowded region prevented us from measuring NOE values with good precision.

In contrast to the heptamer, in the α–β nonamer, no internal motion for each deoxyribose ring was observed. This could be tentatively explained by the increase of the oligonucleotide length (7 base pairs to 9 base pairs) and by the adjonction of the acridine derivative. This fact was already pointed out by Nerdal et al. (1988) on a B-DNA 12-mer. A shorter correlation time (τ = 3.2 ns) was found for the acridine. This could be explained by the equilibrium between both stacked forms of the dye.

The computation of the NOE intensities involving methyl groups has been done by assuming a free rotation of the methyl hydrogens around the C6–C7 bond and using the average of NOE computed for 12 of these positions (Lancelot et al., 1989). The resonances of CH_3 (β-T5) and CH_3 (α-T8) were isochronous and prevented us from determining distances with

these groups. An effective correlation time was calculated for each thymine residue by using the methyl proton–H6 as reference distances and a good agreement was obtained between all the experimental and the calculated CH_3–proton distances (Table VII). However, the discrepancy between the different values of τ proved a different dynamic behavior for each methyl group and was tentatively attributed to a steric hindrance for rotation of some methyl groups. For example for the T3 thymine, the H6–methyl NOEs are abnormally well fitted with $\tau = 5$ ns.

References

Asseline, U., Thuong, N. T., & Hélène, C. (1983) *C. R. Acad. Sci. Ser. 3*, 369–372.

Asseline, U., Delarue, M., Lancelot, G., Toulmé, F., Thuong, N. T., Montenay-Garestier, T., & Hélène, C. (1984) *Proc. Natl. Acad. Sci. U.S.A. 81*, 3297–3301.

Asseline, U., Barbier, C., & Thuong, N. T. (1986) *Phosphorus Sulfur 26*, 63–73.

Barbet, J., Roques, B. P., Combrisson, S., & Le Pecq, J. B. (1976) *Biochemistry 15*, 2642–2650.

Bax, A., & Davis, D. G. (1985) *J. Magn. Reson. 65*, 355–360.

Bodenhausen, G., Vold, R. L., & Vold, R. R. (1980) *J. Magn. Reson. 37*, 93–106.

Borer, P. N., Kan, L. S., & Ts'O, P. O. P. (1975) *Biochemistry 14*, 4864–4875.

Broido, M. S., Zon, G., & James, T. L. (1984) *Biochem. Biophys. Res. Commun. 119*, 663–670.

Cieplak, P., Rao, S. N., Hélène, C., Montenay-Garestier, T., & Kollman, A. (1987) *J. Biomol. Struct. Dyn. 5*, 361–382.

Drobny, G., Pines, A., Sinton, S., Witekamp, D. P., & Wemmer, D. (1979) *Faraday Symp. Chem. Soc. No. 13*, 49–55.

Feigon, J., Leupin, W., Denny, W. A., & Kearns, D. R. (1983) *Biochemistry 22*, 5943–5951.

Feigon, J., Wang, A. H. J., van der Marel, G. A., van Boom, J. H., & Rich, A. (1984) *Nucleic Acids Res. 12*, 1243–1263.

Green, P. J., Pines, O., & Inouye, M. (1986) *Annu. Rev. Biochem. 55*, 559–597.

Guittet, E., Piveteau, D., & Lallemand, J. Y. (1984) *Nucleic Acids Res. 12*, 5827–5941.

Hare, D. R., Wemmer, D. E., Chan, S. H., Drobny, G., & Reid, B. R. (1983) *J. Mol. Biol. 171*, 319–336.

Hélène, C., Montenay-Garestier, T., Saison, T., Takasugi, M., Toulmé, J. J., Asseline, U., Lancelot, G., Maurizot, J. C., Toulmé, F., & Thuong, N. T. (1985) *Biochimie 67*, 777–783.

Hore, P. J. (1983) *J. Magn. Reson. 55*, 283–300.

Jones, T. A. (1978) *J. Appl. Crystallogr. 11*, 268–272.

Lancelot, G., & Thuong, N. T. (1986) *Biochemistry 25*, 5357–5363.

Lancelot, G., Asseline, U., Thuong, N. T., & Hélène, C. (1985) *Biochemistry 24*, 2521–2529.

Lancelot, G., Guesnet, J. L., Roig, V. & Thuong, N. T. (1987) *Nucleic Acids Res. 15*, 7531–7547.

Lancelot, G., Guesnet, J. L., Asseline, U., & Thuong, N. T. (1988) *Biochemistry 27*, 1265–1273.

Lancelot, G., Guesnet, J. L., & Vovelle, F. (1989) *Biochemistry 28*, 7871–7878.

Lavery, R., & Sklenar, H. (1988) *J. Biomol. Struct. Dyn. 6*, 63–91.

Marion, D., & Wüthrich, K. (1983) *Biochem. Biophys. Res. Commun. 113*, 967–874.

Marion, D., & Lancelot, G. (1984) *Biochem. Biophys. Res. Commun. 124*, 774–783.

Morvan, F., Rayner, B., Imbach, J. L., Chang, D. K., & Lown, J. W. (1986) *Nucleic Acids Res. 14*, 5019–5035.

Nerdal, W., Hare, D. R., & Reid, B. R. (1988) *J. Mol. Biol. 201*, 717–739.

Patel, D. J., & Hilberts, C. W. (1975) *Biochemistry 14*, 2651–2660.

Pflugrath, J. W., Saper, M. A., & Quiocho, F. A. (1984) *Methods and Applications in Crystallographic Computing* (Halland, S., & Ashirka, T., Eds.) p 407, Clarendon Press, Oxford.

Sarma, R. H. (1988) *J. Biomol. Struct. Dyn. 6*, 391–395.

Scheek, R. M., Russo, N., Boelens, R., Kaptein, R., & van Boom, J. A. (1983) *J. Am. Chem. Soc. 105*, 2914–2916.

Scheek, R. M., Boelens, R., Russo, N., van Boom, J. H., & Kaptein, R. (1984) *Biochemistry 23*, 1371–1376.

Sun, J. S., Asseline, U., Rouzaud, D., Montenay-Garestier, T., Thuong, N. T., & Hélène, C. (1987) *Nucleic Acids Res. 15*, 6149–6158.

Thuong, N. T., Asseline, U., Roig, V., Takasugi, M., & Hélène, C. (1987) *Proc. Natl. Acad. Sci. U.S.A. 84*, 5129–5133.

Tomazawa, J., & Itoh, T. (1981) *Proc. Natl. Acad. Sci. U.S.A. 78*, 6096–6100.

Weiner, P., & Kollman, P. (1981) *J. Comput. Chem. 2*, 287–303.

Weiner, S. J., Kollman, P. A., Case, D. A., Singh, V. C., Ghio, C., Alagona, G., Profeta, S., & Weiner, P. (1984) *J. Am. Chem. Soc. 106*, 765–784.

Weiss, M. A., Patel, D. J., Sauer, R. T., & Karplus, M. (1984) *Proc. Natl. Acad. Sci. U.S.A. 81*, 130–134.

Wemmer, D. E., Chou, S. H., Hare, D. R., & Reid, B. R. (1984) *Biochemistry 23*, 2262–2265.

Wemmer, D. E., Chou, S. H., Hare, D. R., & Reid, B. R. (1985) *Nucleic Acids Res. 13*, 3755–3772.